LETTERS

Electromagnetic detection of a 410-km-deep melt layer in the southwestern United States

Daniel A. Toffelmier[1] & James A. Tyburczy[1]

A deep-seated melt or fluid layer on top of the 410-km-deep seismic discontinuity in Earth's upper mantle, as proposed in the transition-zone 'water filter' hypothesis[1], may have significant bearing on mantle dynamics and chemical differentiation. The geophysical detection of such a layer has, however, proved difficult. Magnetotelluric and geomagnetic depth sounding are geophysical methods sensitive to mantle melt. Here we use these methods to search for a distinct structure near 410-km depth. We calculate one-dimensional forward models of the response of electrical conductivity depth profiles, based on mineral physics studies of the effect of incorporating hydrogen in upper-mantle and transition-zone minerals. These models indicate that a melt layer at 410-km depth is consistent with regional magnetotelluric and geomagnetic depth sounding data from the southwestern United States (Tucson)[2]. The 410-km-deep melt layer in this model has a conductance of 3.0×10^4 S and an estimated thickness of 5–30 km. This is the only regional data set that we have examined for which such a melt layer structure was found, consistent with regional seismic studies[3]. We infer that the hypothesized transition-zone water filter[1] occurs regionally, but that such a layer is unlikely to be a global feature.

The presence of a melt layer at the base of the upper mantle (410-km depth), as proposed in the transition-zone water filter hypothesis[1], would control water and trace element abundances in the upper mantle as well as indicate a hydrated transition zone. This hypothesis may also explain the differing chemical compositions of ocean island basalts and mid-ocean-ridge basalts[1]. Teleseismically imaged low (seismic) velocity zones have been reported in several areas, and may indicate the existence of a thin melt or fluid layer at this depth in the upper mantle[3,4]. Song *et al.*[3] observe a shear velocity decrease of as much as 5% between 320-km and 410-km depth beneath the western United States. Detection and characterization of this layer could have significant bearing on mantle dynamics, formation and hydration.

Magnetotelluric/geomagnetic depth sounding (MT/GDS) interpretation using mineral physics based electrical conductivity (σ) depth profiles offers the potential for resolving deep upper-mantle features. Using recent measurements on effects of H_2O on the electrical conductivity of upper-mantle and transition-zone minerals[5,6] and melt considerations[7–9], we construct mineral-physics-based electrical conductivity depth profiles of the upper mantle and transition zone consistent with seismic constraints, including the effects of water and a 410-km-deep melt/fluid layer. Forward modelling of the MT/GDS response of these one-dimensional (1D) electrical conductivity depth profiles facilitates characterization of the Earth's electrical response to a 410-km-deep melt layer, and allows comparison to regional MT/GDS field data. Five sufficiently long period ($\geq 10^7$ s), 1D regional MT/GDS data sets were considered in this study (the southern Basin and Range[2], the French Alps[10], North Pacific Ocean[11], a European average[12], and the Canadian Shield[13]).

Electrical conductivity depth profiles are forward modelled following the methods of ref. 14, and are compared to regional MT/GDS data as apparent resistivity, $\rho(\tau)$, and impedance phase, $\varphi(\tau)$, as functions of period, τ. $\rho(\tau)$ and $\varphi(\tau)$ are computed from measured electric and magnetic fields (MT/GDS response) through the complex impedance tensor[15]. The initial electrical conductivity depth profile is calculated using the mineralogy and dry conductivity values of ref. 14 and the geotherm of ref. 16 (see Methods). Then we vary the upper-mantle water content in olivine[5] and the transition zone[6] to minimize the misfit between regional data and forward models, yielding the melt-free regional model. If warranted by transition-zone water content, a high-conductivity (melt) layer is introduced near 410-km depth and the resulting improvement or degradation of the fit is examined.

To determine the sensitivity of the method to a deep upper-mantle melt zone, the MT/GDS response of a 1-km-thick high-conductivity layer of varying conductivity inserted into the initial model is analysed (Fig. 1). The effects of the high-conductivity layer are seen most

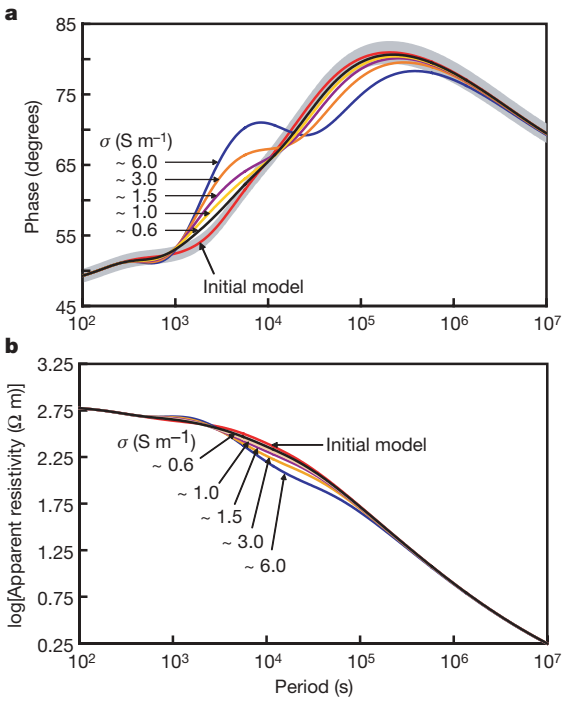

Figure 1 | Forward modelled MT response of upper-mantle conductivity depth profile. Model includes 1-km-thick melt layer at 410-km depth with varying melt electrical conductivity (σ), and illustrates the deviations from the melt-free (initial) model. **a**, $\varphi(\tau)$ models with $\pm 2\%$ error (grey region) on the initial model, and **b**, $\rho(\tau)$. The initial model is described in the Methods.

[1]School of Earth and Space Exploration, Arizona State University, Tempe, Arizona 85287-1404, USA.

clearly in the $\varphi(\tau)$ response between periods of 10^3 and 10^5 s. Assuming a 2% error in the $\varphi(\tau)$ data in the 10^3–10^5 s range, a 1-km-thick layer with conductivity greater than 1.0 S m^{-1} ($\geq$2.25 log units conductivity above the conductivity of the upper mantle at 409-km depth) could be detectable by MT/GDS methods (in agreement with χ^2 arguments, see Supplementary Information). Performing this analysis for high-conductivity layers of differing thickness gives an effective minimum conductance of ~1,000 S for a detectable high-conductivity layer near 410-km depth. The effective minimum conductance is dependent on the surrounding mantle conductivity structure and may vary regionally (see Supplementary Information).

In the transition-zone water filter hypothesis[1], a 410-km-deep melt layer may be composed of mafic material and contain high concentrations of incompatible elements. The melt may be hydrated and denser than the surrounding upper mantle, allowing the formation of a stable melt layer atop the 410-km-deep seismic discontinuity. Because the composition of a 410-km-deep melt is uncertain, the electrical conductivities of various melts are considered (Fig. 2). Electrical conductivity of silicate melts decreases with increasing pressure up to 2 GPa; at greater pressure, the dependence is reduced[9]. The electrical conductivity of basaltic melt at 1,420 °C and 2.5 GPa is ~6.0 S m^{-1}, whereas for rhyolitic melt it is ~2.0 S m^{-1} (ref. 8). Alternative compositions such as (Mg,Fe)O fluids may be possible in this depth range, but experimental verification is lacking. Supercritical H_2O may also be possible; shock experiments yield electrical conductivity of ~100 S m^{-1} at 15 GPa and ~1,000 °C (ref. 17).

At pressure–temperature conditions near 410-km depth, mafic melt is denser than olivine[18–20]. It is not known whether fluids/melts of (Mg,Fe)O compositions would be gravitationally stable at these conditions. Shock experiments indicate that at the pressure–temperature conditions near 410-km depth, supercritical H_2O may be less dense than olivine[17] and unable to form a stable layer. H_2O added to a silicate melt decreases its density[21] and may increase its electrical conductivity[7]. A mafic melt at 410-km depth will remain denser than the surrounding upper mantle if it contains less than ~6.0 wt% H_2O (refs 21, 22). The electrical conductivity enhancement for 6.0 wt% H_2O in a rhyolitic melt is ~0.25 log units above that of a dry rhyolitic melt[7]. The effects of water on the electrical conductivity of mafic melts are unknown. We use an electrical conductivity of ~6.0 S m^{-1} as that of a melt near 410-km depth in calculations of layer thickness.

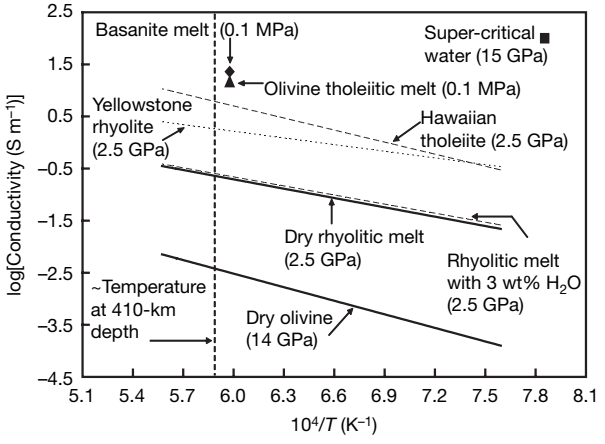

Figure 2 | Electrical conductivity of various melts as a function of inverse temperature. Upper solid line, rhyolitic melt at 2.5 GPa (ref. 7); nearby dashed line, rhyolitic melt with 3.0 wt% H_2O at 2.5 GPa (ref. 7); short-dashed line, Yellowstone rhyolite obsidian[9] at 2.5 GPa; long-dashed line, Hawaiian tholeiite[9] at 2.5 GPa. Square, supercritical water at 1,000 °C and 15 GPa (ref. 17). Triangle and diamond represent olivine tholeiitic melt[9] and basanite[8] at 0.1 MPa and ~1,400 °C, respectively. Also plotted is electrical conductivity of isotropic olivine[14] for comparison (lower solid line). Vertical dashed line indicates approximate temperature at 410-km depth (~1,420 °C).

To allow upper-mantle melting, upwelling material (from the transition zone) must be sufficiently hydrated. Assuming that the H_2O storage capacity of the upper mantle is controlled by olivine alone, solubility measurements indicate a storage capacity of ~0.4 wt% H_2O (6.5×10^4 H per 10^6 Si, equivalent to 3.27 mol% H_2O) at 1,100 °C and 12 GPa (refs 23, 24; see Supplementary Information). Accounting for H_2O partitioning between olivine and other mantle minerals, upper-mantle H_2O storage capacity could be between 0.4 and 0.55 wt% H_2O at 410-km depth[25]. Upper-mantle melting may occur only when the transition zone contains more water than the upper mantle can stably sequester; 0.4 wt% H_2O is chosen as the minimum amount of water needed in the transition zone to induce upper-mantle melting. The maximum solubility of H_2O in transition-zone minerals is ~3.0 wt% at similar pressure–temperature conditions[23], indicating that the transition zone can accommodate sufficient H_2O to supersaturate the upper mantle through upwelling events.

The southern Basin and Range region near Tucson, Arizona, is characterized by slow seismic wave speeds in the upper mantle (the upper 100–200 km) and fast wave speeds in the transition zone (500–900 km depth)[26]. A low-velocity zone has been seismically imaged in the western US, for which a 20–90-km-thick partial melt layer was inferred at the base of the upper mantle (410 km depth)[3]. Physical observations of the southern Basin and Range suggest lateral heterogeneities in the shallow lithosphere and a 1D upper mantle and transition zone. To determine if the Tucson MT/GDS data set is sufficiently 1D, the D^+ inversion[27] is used[2,27]. The D^+ inversion, while not a physical model, will yield the minimum χ^2 misfit for a 1D solution[27]. If the χ^2 misfit of the D^+ inversion is nearly equal to the degrees of freedom (d.f.) of the data set, then the data are sufficiently 1D in nature. The D^+ models of the Tucson data yield $\chi^2 = 62$ (d.f. = 48), indicating that the data set is nearly 1D. The smooth inversion of the data of ref. 2 yields $\chi^2 = 74$. The melt-free regional conductivity versus depth model includes 0.23 wt% H_2O in upper-mantle olivine (to 410-km depth) and 0.6 wt% H_2O in the transition zone, yielding $\chi^2 = 128$. Addition of a high-conductivity layer at 410-km depth is warranted because the transition-zone water content in this model is greater than 0.4 wt% H_2O. The water content estimate for the transition zone depends on the transition-zone geotherm. The geotherm used in ref. 14 is 50–75 °C hotter than that of ref. 16 in the transition zone. This hotter geotherm reduces the transition-zone water content to 0.40 wt% H_2O for the Tucson data, which reaches the threshold for requiring a melt zone at 410-km depth. Minimizing χ^2 in the model including melt results in a melt layer with a conductance of $\sim 3.0 \times 10^4$ S, and improves the χ^2 to 70 (Fig. 3). A melt layer of pure mafic melt ($\sigma \approx 6.0$ S m^{-1}) with a conductance of $\sim 3.0 \times 10^4$ S would be ~5-km thick. Considering resolution constraints (see Supplementary Information), we estimate that the melt (or partial melt) layer in this region is 5–30 km thick, in agreement with the teleseismic study of Song *et al.*[3]

Similar analyses of other regional data sets[10–13] confirm that the mineralogy[14] and geotherm[16] used are in good agreement with field data. The regional conductivities are consistent with 0.003 and 0.010 wt% H_2O (upper mantle and transition zone, respectively) in the French Alps[10], 0.12 and 0.20 wt% H_2O in the North Pacific[11], 0.11 and 0.15 wt% H_2O for the European average[12], and 0.02 and 0.15 wt% H_2O in the Canadian Shield[13]. These values are not consistent with a transition-zone water content greater than 0.4 wt% H_2O, therefore melt layers in these regions are not warranted. Disregarding water solubility arguments and adding high-conductivity layers into these regional models resulted in no significant reduction of χ^2 and in most cases required a significant reduction of the surrounding mantle conductivity (compared to the melt-free regional model) to maintain the model fit to the data

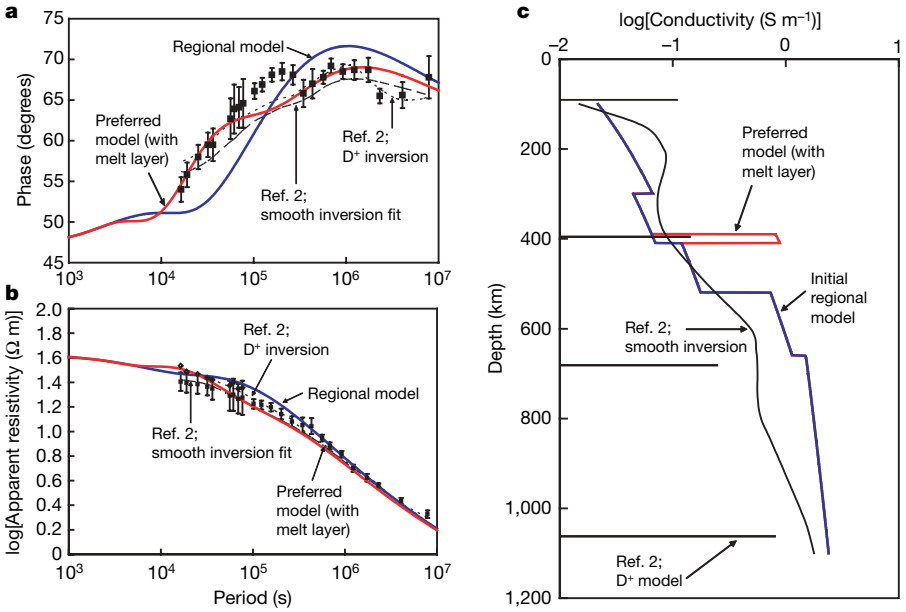

Figure 3 | Forward modelling results for the southern Basin and Range (Tucson) data set[2]. The smoothed inversion of ref. 2 is the long-dashed line; the short-dashed line is the D^+ inversion[2]. The red line is the preferred model with melt layer; the blue line is the melt-free 'regional' model. **a**, $\varphi(\tau)$ models, and **b**, $\rho(\tau)$ models with the original data (black squares) and calculated upward biased $\rho(\tau)$ data (diamonds)[2]. Error bars are the modified error bars of ref. 2, corresponding to $\pm 1\sigma$ except where noted. **c**, Electrical conductivity depth profiles.

(Supplementary Information and Supplementary Fig. 1). The requirement to reduce the electrical conductivity of the mantle above and below the high-conductivity layer indicates that a high-conductivity zone is not a robust feature of these regions. The models best fitting the Tucson[2] data did not require a reduction in the electrical conductivity of the surrounding mantle, suggesting that a high-conductivity layer at 410-km depth is robust feature of the data.

1D forward modelling of MT/GDS responses of electrical conductivity depth profiles created using seismic and mineral physics constraints indicates that electrical methods can be used as imaging tools to detect thin conductive zones at 410-km depth. The estimated minimum detectible conductance for a high-conductivity layer at 410-km depth is ~1,000 S; however, this may vary regionally, depending on the surrounding electrical conductivity structure. The agreement between forward models and southern Basin and Range (Tucson)[2] MT/GDS data is enhanced when a melt layer at 410-km depth is added to the hydrogen-containing mineralogically based regional electrical conductivity depth profile, and is consistent with petrologic constraints on hydrogen-enhanced melting at these depths. This is the only region studied where this is the case. A melt (or partial melt) layer with conductance of $\sim 3.0 \times 10^4$ S (5–30 km thick) is in agreement with seismic studies[3]. These results do not support the global presence of a transition-zone water filter, but instead indicate its regional occurrence. Additional long-period MT/GDS field studies and stricter limits on melt composition and conductivity are needed to constrain the existence and properties of a 410-km-deep melt layer.

METHODS

The mineralogy of all models is based on that of ref. 14 with 60 vol.% olivine, 25 vol.% orthopyroxene and 15 vol.% clinopyroxene between 100-km and 300-km depth. Between 300-km and 410-km depth, the profile consists of 60 vol.% olivine and 40 vol.% clinopyroxene. The upper transition zone (410–520 km depth) is composed of 60 vol.% wadsleyite and 40 vol.% clinopyroxene. The lower transition zone (520–660km depth) is composed of 60 vol.% ringwoodite and 40 vol.% akimotoite plus garnet. The lower mantle is composed of 75 vol.% Al-bearing perovskite (~2.9 wt% Al) and 25 vol.% magnesiowüstite. The geotherm of ref. 16 is used as the temperature profile for all models. A regional conductivity profile is created by adding water to olivine[5] in the upper mantle and to wadsleyite and ringwoodite[6] in the transition zone to better fit specific regional MT/GDS field responses (that is, the melt-free regional model, blue line in Fig. 3). If the response indicates transition-zone conductivity consistent with transition-zone minerals having $\geq$0.4 wt% H_2O, then a high-conductivity (melt) layer is added to the model (red line in Fig. 3).

Received 25 January; accepted 10 May 2007.

1. Bercovici, D. & Karato, S. Whole-mantle convection and the transition-zone water filter. *Nature* **425**, 39–44 (2003).
2. Egbert, G. D., Booker, J. R. & Schultz, A. Very long period magnetotellurics at Tucson Observatory: Estimation of impedances. *J. Geophys. Res. B* **97**, 15113–15128 (1992).
3. Song, T. R. A., Helmberger, D. V. & Grand, S. P. Low-velocity zone atop the 410-km seismic discontinuity in the northwestern United States. *Nature* **427**, 530–533 (2004).
4. Revenaugh, J. & Sipkin, S. A. Seismic evidence for silicate melt atop the 410-km mantle discontinuity. *Nature* **369**, 474–476 (1994).
5. Wang, D., Mookherjee, M., Xu, Y. S. & Karato, S. The effect of hydrogen on the electrical conductivity in olivine. *Nature* **443**, 977–980 (2006).
6. Huang, X. G., Xu, Y. S. & Karato, S. I. Water content in the transition zone from electrical conductivity of wadsleyite and ringwoodite. *Nature* **434**, 746–749 (2005).
7. Gaillard, F. Laboratory measurements of electrical conductivity of hydrous and dry silicic melts under pressure. *Earth Planet. Sci. Lett.* **218**, 215–228 (2004).
8. Tyburczy, J. A. & Fisler, D. K. in *Mineral Physics and Crystallography: A Handbook of Physical Constants* (ed. Ahrens, T. J.) 185–208 (American Geophysical Union, Washington DC, 1995).
9. Tyburczy, J. A. & Waff, H. S. Electrical conductivity of molten basalt and andesite to 25 kilobars pressure — Geophysical significance and implications for charge transport and melt structure. *J. Geophys. Res.* **88**, 2413–2430 (1983).
10. Tarits, P., Hautot, S. & Perrier, F. Water in the mantle: Results from electrical conductivity beneath the French Alps. *Geophys. Res. Lett.* **31**, L06612, doi:10.1029/2003GL019227 (2004).
11. Lizarralde, D., Chave, A., Hirth, G. & Schultz, A. Northeastern Pacific mantle conductivity profile from long-period magnetotelluric sounding using Hawaii-to-California submarine cable data. *J. Geophys. Res. B* **100**, 17837–17854 (1995).
12. Olsen, N. Long-period (30 days-1 year) electromagnetic sounding and the electrical conductivity of the lower mantle beneath Europe. *Geophys. J. Int.* **138**, 179–187 (1999).
13. Schultz, A., Kurtz, R. D., Chave, A. D. & Jones, A. G. Conductivity discontinuities in the upper mantle beneath a stable craton. *Geophys. Res. Lett.* **20**, 2941–2944 (1993).
14. Xu, Y. S., Shankland, T. J. & Poe, B. T. Laboratory-based electrical conductivity in the Earth's mantle. *J. Geophys. Res. B* **105**, 27865–27875 (2000).
15. Simpson, F. Resistance to mantle flow inferred from electromagnetic strike of the Australian upper mantle. *Nature* **412**, 632–635 (2001).

16. Brown, J. M. & Shankland, T. J. Thermodynamic parameters in the Earth as determined from seismic profiles. *Geophys. J. R. Astron. Soc.* **66,** 579–596 (1981).
17. Mitchell, A. C. & Nellis, W. J. Equation of state and electrical conductivity of water and ammonia shocked to 100 GPa (1Mbar) pressure range. *J. Chem. Phys.* **76,** 6273–6281 (1982).
18. Ohtani, E. & Maeda, M. Density of basaltic melt at high pressure and stability of the melt at the base of the lower mantle. *Earth Planet. Sci. Lett.* **193,** 69–75 (2001).
19. Ohtani, E., Nagata, Y., Suzuki, A. & Kato, T. Melting relations of peridotite and the density crossover in planetary mantles. *Chem. Geol.* **120,** 207–221 (1995).
20. Suzuki, A., Ohtani, E. & Kato, T. Density and thermal expansion of a peridotite melt at high pressure. *Phys. Earth Planet. Inter.* **107,** 53–61 (1998).
21. Matsukage, K. N., Jing, Z. C. & Karato, S. Density of hydrous silicate melt at the conditions of Earth's deep upper mantle. *Nature* **438,** 488–491 (2005).
22. Sakamaki, T., Suzuki, A. & Ohtani, E. Stability of hydrous melt at the base of the Earth's upper mantle. *Nature* **439,** 192–194 (2006).
23. Kohlstedt, D. L., Keppler, H. & Rubie, D. C. Solubility of water in the α, β and γ phases of $(Mg,Fe)_2SiO_4$. *Contrib. Mineral. Petrol.* **123,** 345–357 (1996).
24. Bell, D. R., Rossman, G. R., Maldener, J., Endisch, D. & Rauch, F. Hydroxide in olivine: A quantitative determination of the absolute amount and calibration of the IR spectrum. *J. Geophys. Res.* **108,** B2105, doi:10.1029/2001JB000679 (2003).
25. Hirschmann, M. M., Aubaud, C. & Withers, A. C. Storage capacity of H_2O in nominally anhydrous minerals in the upper mantle. *Earth Planet. Sci. Lett.* **236,** 167–181 (2005).
26. van der Lee, S. & Nolet, G. Upper mantle S velocity structure of North America. *J. Geophys. Res. B* **102,** 22815–22838 (1997).
27. Parker, R. L. The inverse problem of electromagnetic induction — Existence and construction of solutions based on incomplete data. *J. Geophys. Res.* **85,** 4421–4428 (1980).

Supplementary Information is linked to the online version of the paper at www.nature.com/nature.

Acknowledgements We thank S. Constable and E. Garnero for comments and discussion. This work was supported by the National Science Foundation.

Author Information Reprints and permissions information is available at www.nature.com/reprints. The authors declare no competing financial interests. Correspondence and requests for materials should be addressed to J.A.T. (jim.tyburczy@asu.edu).